SPREAD OF SMOKE AND HEAT ALONG NARROW AIR CAVITY IN DOUBLE-SKIN FAÇADE FIRES

by

Cheuk Lun CHOW*

Department of Architecture, Wolfson College, University of Cambridge, UK*

Original scientific paper
DOI: 10.2298/TSCI110918094C

A scenario on double-skin façade fire was identified earlier for hazard assessment. A flashover room fire occurred next to the façade, broke the interior glass pane and spread to the façade cavity. As observed in experiments, hot gas moved up as a vertical channel flow for narrow façade cavity. Heat and smoke spread along the narrow air cavity of a double-skin façade will be studied in this paper. A simple mathematical model is developed from basic heat transfer theory for studying the vertical air temperature profiles of the hot gas flowing along the cavity. Assuming one-dimensional flow for hot gas moving up the façade cavity, conservation equations on mass and enthalpy were solved. Experimental results on two double-skin façade rigs of height 6 m and 15 m with narrow cavity depth were used to justify the results. A total of 11 tests were carried out. Correlation expressions between cavity air temperature and the height above ceiling of the fire room were derived.

Key words: *smoke, heat, double-skin façade, fire hazard*

Introduction

Buildings with glass façades would give better views and admit more daylight [1]. The buildings can be constructed relatively quickly at lower construction cost. However, the cooling load of those buildings in tropical areas is very high. Double-skin façades (DSF) are proposed [2-4] to reduce the solar heat gain in glazed walls and for environmental benefits. DSF is an architectural feature with two layers of glass façade built in parallel developed on the concept of the traditional box-type window. The air gap between the outer casement and the inner glazing can be extended vertically through several floors or even the entire building height. The façade cavity works as a buffer zone to give better thermal insulation. It is able to serve as an air ventilation channel depending on the need of occupants. This architectural feature on façade design is different from a double-glazing system, where the distance between the two glass panes can be as much as 2 m. DSF designs are becoming popular in the Far East.

Fire hazard in glass architectural feature [5, 6] is, however a concern. Many buildings with DSF, particularly those with multi-floors high cavity, have difficulties in complying with the fire regulations in those big cities, particularly in East Asia including China Mainland, Hong Kong, Korea, Japan, Singapore, Malaysia, Thailand, and Taiwan. The current fire codes on curtain walled buildings in those cities are very limited, and not demonstrated to work in a fire. Taking Hong Kong as an example, only "normal requirements" [7] are speci-

* Now at: Department of Civil and Architectural Engineering, City University of Hong Kong
Author's e-mail: beelize@polyu.edu.hk; cheuhow@cityu.edu.hk

fied on curtain walled buildings with over six floors. Fire codes on glass façades in other countries are also limited with some studies just started in Japan [8]. Additional fire safety provisions are required, but it is not yet demonstrated that providing the specified hardware provisions, such as a vertical spandrel of height over 900 mm in Hong Kong, can give appropriate safety to the identified scenario. Therefore, fire safety for DSF [5, 6, 9, 10] should be studied in more detail to recommend appropriate measures for the codes.

As identified before [11, 12], a post-flashover room fire occurred next to the DSF would spread flame and smoke to the façade cavity through those openings resulted from broken glass panes. For narrow cavity depths, hot gas would spread up as a channel flow along the cavity. The vertical air temperature did not fall rapidly with height while moving up the narrow façade cavity. These results are shown clearly in the vertical temperature profiles from full-scale burning tests [11]. The vertical channel flow of hot gas along the façade cavity will be studied in this paper by a single mathematical model.

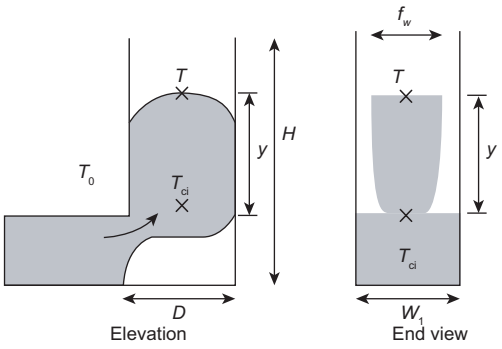

Figure 1. Schematic diagram

The mathematical model

Hot gases with density ρ, upward velocity v, and temperature T flowing out of a post-flashover room fire to the DSF feature with a channel geometrical factor G was approximated by a 1-D model along the height above the fire room ceiling y as in fig. 1. Neglecting flow resistance with the façade wall, conservation equations on mass and enthalpy [13-18] are:

$$\frac{\partial \rho}{\partial t} + \frac{\partial (\rho v)}{\partial y} = 0 \tag{1}$$

$$\rho C_p \left(\frac{\partial T}{\partial t} + v \frac{\partial T}{\partial y} \right) = -k \frac{\partial^2 T}{\partial y^2} + \frac{h}{4G}(T_0 - T) \tag{2}$$

In the above thermal equation, k is the thermal conductivity, h – the heat transfer coefficient, and T_0 – the initial and ambient temperature.

Ideal gas law gives the relation between T at height y, T_0 and the ambient air pressure P_0 in terms of gas constants R, molar mass M and R^* (given by RM):

$$\rho T = \rho_0 T_0 = \frac{P_0}{RM} = \frac{P_0}{R^*} = \text{Constant} \tag{3}$$

The channel geometrical factor G depends on the cavity depth D and a factor describing the width of the channel flow W_1 as:

$$G = \frac{2DW_1}{D + W_1} \tag{4}$$

The value of W_1 can be taken as the opening window flame width f_w ejected out of the opening and assumed to be constant for simple analysis. In this way, G is also a constant.

Note that the mass flow rate $\dot{m}$ can be calculated by density, velocity, and cross-sectional area A across the hot gas as ρvA and can be taken to be constant. Putting in eq. (3) gives:

$$\frac{v}{T} = \frac{\dot{m}}{A}\frac{R^*}{P_0} = I \tag{5}$$

Note that I is a parameter which depends only on initial conditions, channel geometry, and horizontal cross-sectional area of hot gas. Rearranging eq. (2) with those constants gives the thermal equation under steady temperature state as:

$$\frac{\mathrm{d}T}{\mathrm{d}y} = \frac{-k}{I\rho_0 T_0 C_p}\frac{\mathrm{d}^2T}{\mathrm{d}y^2} + \frac{h}{4GI\rho_0 T_0 C_p}(T_0 - T) \tag{6}$$

Transforming the above into dimensionless forms with quantities θ, ϕ, and Y in terms of height of façade rig H:

$$\theta = \frac{T - T_0}{T_0}, \quad \phi = \frac{\rho_0 - \rho}{\rho_0}, \quad Y = \frac{y}{H} \tag{7}$$

The key thermal eq. (6) becomes:

$$\frac{k}{HI\rho_0 C_p T_0}\frac{\mathrm{d}^2\theta}{\mathrm{d}Y^2} + \frac{\mathrm{d}\theta}{\mathrm{d}Y} + \frac{Hh}{4GI\rho_0 C_p T_0}\theta = 0 \tag{8}$$

This is a second-order ordinary differential equation which can be expressed in terms of two parameters β_1 and γ:

$$\frac{\mathrm{d}^2\theta}{\mathrm{d}Y^2} + \frac{1}{\gamma}\frac{\mathrm{d}\theta}{\mathrm{d}Y} + \frac{\beta_1}{\gamma}\theta = 0 \tag{9}$$

where

$$\beta_1 = \frac{Hh}{4GI\rho_0 C_p T_0}, \quad \gamma = \frac{k}{HI\rho_0 C_p T_0} \tag{10}$$

The ratio of γ/β_1 is therefore:

$$\frac{\gamma}{\beta_1} = \frac{4Gk}{H^2 h} \tag{11}$$

Convection across a vertical plane [19] would give a dimensionless Nusselt number Nu expressed in terms of h and k as:

$$\mathrm{Nu} = \frac{hH}{k} \tag{12}$$

The value of h is roughly constant but value of k depends on temperatures, taking values of 0.0263 W/mK at 300 K and 0.0338 W/mK at 450 K. Value of Nu is about 1000 for fire-driven flow fields. Putting the above expression (12) for Nu to γ/β_1 gives:

$$\frac{\gamma}{\beta_1} = \frac{4G}{H\mathrm{Nu}} \tag{13}$$

Solution of the thermal equation

The boundary condition θ_0 at $Y = 0$ depends on the ceiling jet temperature moving out of the room T_{ci} as in fig. 1:

$$\theta_0 = \frac{T_{ci} - T_0}{T_0} \tag{14}$$

The solution for eq. (9) under this boundary condition (14) is:

$$\theta = C_1 \mathrm{e}^{m_1 Y} + C_2 \mathrm{e}^{m_2 Y} \tag{15}$$

where m_1 and m_2 are solutions of m in the following quadratic equation:

$$m^2 + \frac{m}{\gamma} + \frac{\beta_1}{\gamma} = 0 \tag{16}$$

There are two real roots of m_1 and m_2 when the discriminant of the above quadratic equation on m is greater than zero. If m_1 and m_2 are real and distinct roots in addition to θ_0, another boundary condition is required. Roots m_1 and m_2 will be complex numbers when the discriminant is less than zero. In this paper, only roots of the quadratic equation are considered.

Taking $\mathrm{d}\theta/\mathrm{d}Y$ to θ'_0 at $Y = 0$ gives a solution to the thermal eq. (9) under the boundary condition (14) is:

$$\theta = \left[\frac{(\sqrt{1-4\gamma\beta_1}+1)\theta_0 + 2\gamma\theta'_0}{2\sqrt{1-4\gamma\beta_1}}\right]\mathrm{e}^{\frac{\sqrt{1-4\gamma\beta_1}-1}{2\gamma}Y} + \left[\frac{(\sqrt{1-4\gamma\beta_1}-1)\theta_0 - 2\gamma\theta'_0}{2\sqrt{1-4\gamma\beta_1}}\right]\mathrm{e}^{-\frac{\sqrt{1-4\gamma\beta_1}+1}{2\gamma}Y} \tag{17}$$

Note that $\gamma\beta_1$ is:

$$\gamma\beta_1 = \frac{hk}{4GI^2\rho_0{}^2 C_p{}^2 T_0{}^2} \tag{18}$$

Value of $\gamma\beta_1$ is much less than 1 as verified by putting in numerical values of parameters concerned, giving $1 - 4\gamma\beta_1$ to be about 1. The solution can then be simplified as:

$$\theta = \theta_0 + \gamma\theta'_0(1 - \mathrm{e}^{-Y/\gamma}) \tag{19}$$

If m_1 and m_2 are identical roots, the discriminant in eq. (16) is 0 and $4\gamma\beta_1$ is 1. This gives:

$$m_1 = m_2 = m = -1/2\gamma = 2\beta_1 \tag{20}$$

and

$$\theta = C_1 \mathrm{e}^{mY} + C_2 Y \mathrm{e}^{mY} \tag{21}$$

When $4\gamma\beta_1$ is 1, only one boundary condition of $\theta = \theta_0$ at $Y = 0$ is required to solve for the second-order differential eq. (9) to give:

$$\theta = \theta_0(1 + 2\beta Y)\mathrm{e}^{-2\beta_1 Y} \tag{22}$$

or

$$\theta = \theta_0\left(1 + \frac{Y}{2\gamma}\right)\mathrm{e}^{-Y/2\gamma} \tag{23}$$

Another common practice [*e. g.* 18] to solve eq. (9) is to ignore the second derivative. This is justified by taking $d^2\theta/dY^2$ to be very small and tends to zero; or when γ is much less than β_1.

Equation (9) becomes:

$$\frac{d\theta}{dY} + \beta_1\theta = 0 \tag{24}$$

Direct integration from 0 to Y gives:

$$\theta = \theta_0 e^{-\beta_1 Y} \tag{25}$$

Equation (17) is a general solution to (9) to give the vertical air temperature profile under steady temperature state. However, the expression is rather complicated. Equation (19) is the simplification of the solution to (9) when $\gamma\beta_1$ is much less than 1. Equation (23) holds when $4\gamma\beta_1$ is 1. Equation (25) was derived by neglecting the second-order derivative in eq. (9), or when γ is much less than β_1.

Putting back eq. (25) into dimensional form as in y and T would give the steady vertical air temperature T at different heights y:

$$\frac{T - T_0}{T_0} = \left(\frac{T_{ci} - T_0}{T_0}\right) e^{-\frac{\beta_1 y}{H}}, \quad \Delta T = (T_{ci} - T_0)\, e^{-\frac{\beta_1 y}{H}} \tag{26}$$

Curves on the four particular solutions

The parameters in eqs. (17), (19), (23), and (25) are rather complicated, but can be derived by statistical analysis using experimental data. The following four curves are fitted for different particular solutions:

– *Curve 1*

Equation (25) is the solution to eq. (9) solved by neglecting the second-order derivative or for $\gamma \ll \beta_1$. It is labeled as curve 1 and can be rewritten as:

$$\theta = A_1 e^{-C_1 Y} \tag{27}$$

where

$$A_1 = \theta_0, \quad C_1 = \beta_1 \tag{28}$$

Denoting $T_{ci} - T_0$ in eq. (14) as the ceiling jet temperature rise ΔT_{CJ} for hot gases flowing out of the room:

$$\Delta T_{CJ} = T_{ci} - T_0 \tag{28b}$$

Equation (27) can be deduced by estimating ΔT at height y:

$$\ell n \Delta T = \ell n \Delta T_{CJ} - \frac{\beta_1 y}{H} \tag{28c}$$

– *Curve 2*

Rewrite the solution of θ for $\gamma\beta_1 \ll 1$ given by eq. (19) as:

$$\theta = A_2 - B_2 e^{-C_2 Y} \tag{29}$$

where

$$A_2 = \theta_0 + \gamma\theta_0', \quad B_2 = \gamma\theta_0', \quad C_2 = -\frac{1}{\gamma} \tag{30}$$

– *Curve 3*

Rewrite the solution of θ when $4\gamma\beta_1 = 1$ given by eq. (23):

$$\theta = (A_3 + B_3 Y)\mathrm{e}^{-C_3 Y} \tag{31}$$

where

$$A_3 = \theta_0, \quad B_3 = 2\beta_1\theta_0 = \frac{\theta_0}{2\gamma}, \quad C_3 = 2\beta_1 = \frac{1}{2\gamma} \tag{32}$$

– *Curve 4*

Rewrite the general solution of θ without ignoring any terms given by eq. (17) as:

$$\theta = A_4\mathrm{e}^{C_4 Y} + B_4\mathrm{e}^{C_5 Y} \tag{33}$$

where A_4, B_4, C_4, and C_5 are complicated expressions.

The correlations between θ and Y at steady temperature state from eqs. (27), (29), (31), and (33) can be deduced by the method of least square fitting [20, 21] on experimental data.

Statistical analysis with experimental data

Full-scale experiments [11] with the scenario on part of a multistory DSF were carried out at the burning site at Harbin, Heilongjiang, China. Two DSF rigs were constructed to study the fire scenario identified. A 6 m tall DSF feature labeled as DS was constructed first as in fig. 2(a) in 2007. That rig was not tall enough to study the vertical channel flow completely. Another taller DSF rig labeled as DSN of height 15 m as shown in fig. 2(b) was then constructed in 2008. A cavity was enclosed by two panels (made of glass panes, timber chip-

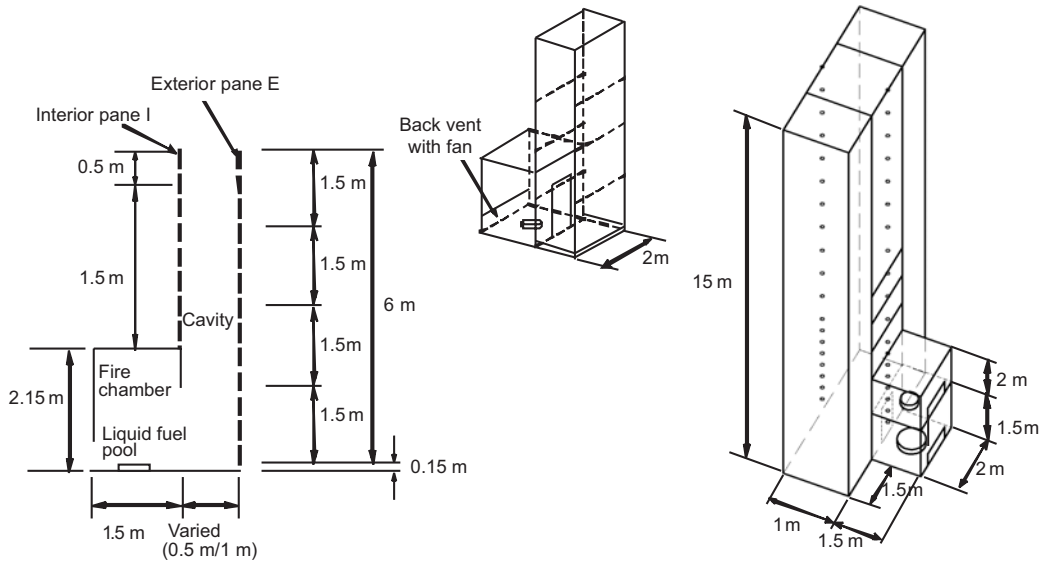

(a) Rig DS in 2007 (b) Rig DSN in 2008

Figure 2. DSF rigs

board or steel sheets) in parallel as shown in the figure. A fire chamber was placed next to it to direct flame out to act at the DSF rigs. The size of the fire chamber is also shown in the figure. A 0.81 m diameter pool fire with 10,000 ml gasoline was placed in the chamber for two rigs. The heat release rate of the pool fire was up to 1.2 MW and burning duration about 500 s. A fan was operated to drive flame out of the room. Air temperature differences in positions adjacent to the interior and exterior glass panes inside the cavity were measured to justify the four curves on vertical air temperature profile derived as in above. Details of these burning tests were reported before and will not be repeated here [11].

Table 1. Full-scale burning tests

DSF rig	Test number	Cavity depth [m]	Construction materials
DS	DS-1-a	1.0	All glass panes
	DS-1-b		
	DS-1-c	1.0	Three sides of steel sheet and one side glass pane
	DS-1-d		
	DS-2-a	0.5	
	DS-2-b		
DSN	DSN-1-a	1.0	All glass panes
	DSN-1-b		
	DSN-1-c		
	DSN-1-d	1.0	All timber chipboards
	DSN-1-e		

Six tests carried out in the DSF rig DS of 6 m tall and five tests in the taller rig DSN of 15 m tall were taken out. These tests were labeled as DS-1-a, DS-1-b, DS-1-c, and DS-1-d for 1 m cavity depth; DS-2-a and DS-2-b for 0.5 m cavity depth for DS; and DSN-1-a to DSN-1-e in DSN for 1 m cavity depth. A summary is shown in tab. 1.

The air temperature profiles measured in the façade cavity of the two rigs are shown in figs. 3 and 4. Results are used to justify eqs. (27), (29), (31), and (33).

The proportion of variability explained by the fitted curve as in the equations can be measured by the coefficient of determination R^2. The fit is perfect if R^2 is 1 and poor for R^2 approaching 0. A value of 0.9 indicates that 90% of the variables surveyed can be explained by the fitted equation. The square root of R^2 is the correlation coefficient. Again, the value of R near to 1 or –1 indicates excellent correlation; approaching 0 means poor correlation.

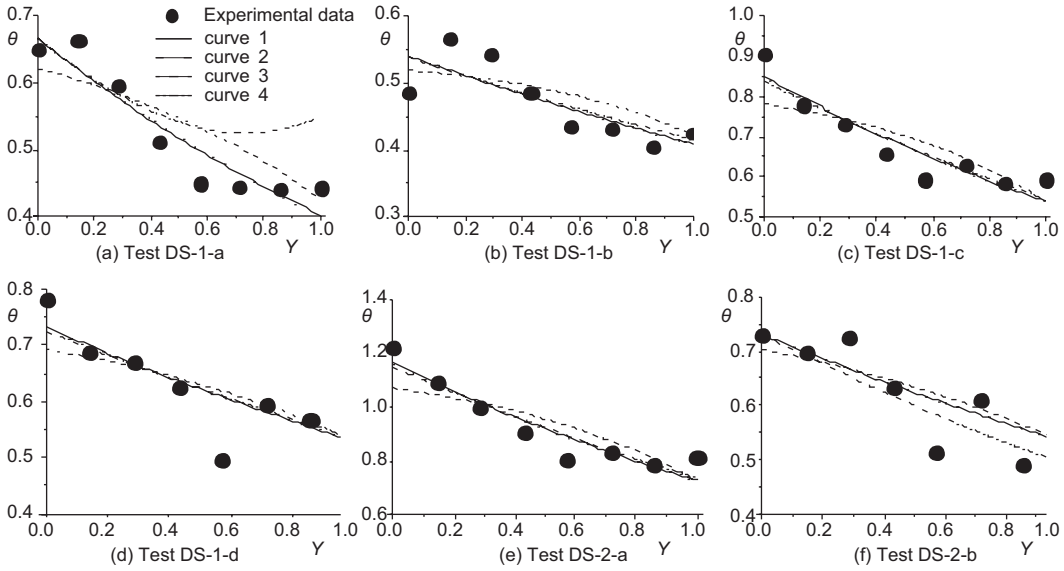

Figure 3. Curves fitted in tests for 6 m tall DS rig

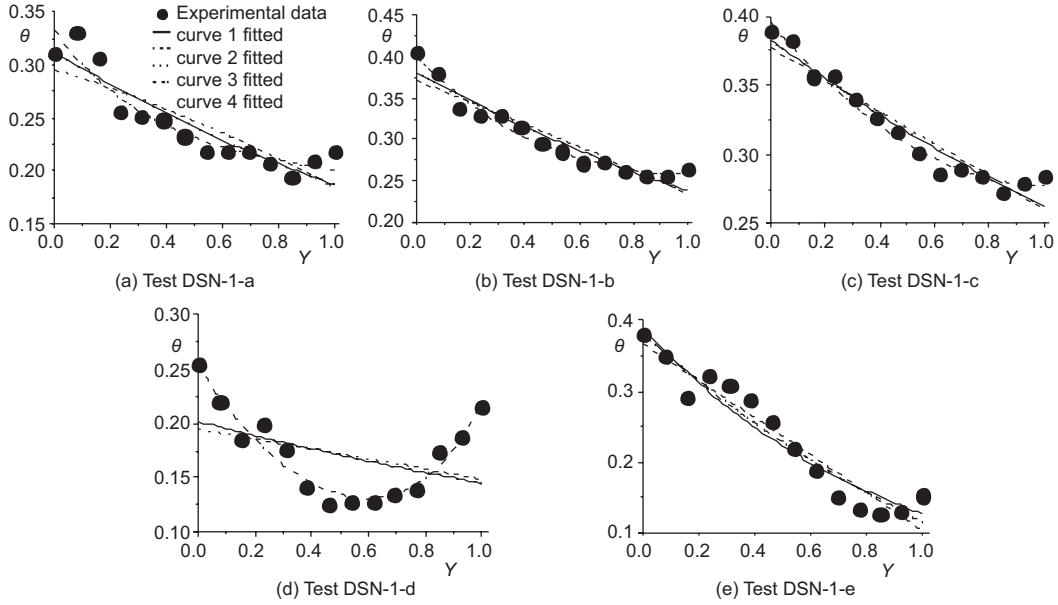

Figure 4. Curves fitted in tests for 15 m tall DSN rig

Discussions

Results on fitting parameters in the tests DS-1-a to DS-1-d, DS-2-a and DS-2-b in DSF rig DS; and DSN-1-a to DSN-1-e in the taller rig DSN are shown in tab. 2 for the curves 1 to 4. All four curves 1 to 4 are plotted in fig. 3 for tests in the DSF rig DS; and in fig. 4 for tests in the rig DSN.

Curve 1 in steady temperature state is fitted for air temperature at the façade cavity with coefficient of determination R^2 shown in tab. 2. ΔT for curve 1 was fitted by two ways:

(1) The intercept is fixed to the measured value of ΔT_{CJ}. Only the slope of the line is fitted.

(2) Both the slope and the intercept were fitted by correlation analysis.

Although values of R^2 for the correlation relations on T_M are reasonably high with value up to 0.94 for test DSN-1-c, test DSN-1-d gave a negative value of R^2 for fixed intercept. Further, measured results of tests DSN-1-d and DSN-1-e are different due to short burning time for test DSN-1-e.

Note that for fitting the lines with fixed intercepts, R^2 might be very small and even less than zero. That is because coefficients in the linear equation with imposed parameters were not entirely fitted by least square. The fixed intercept even gives negative value (–0.19 for DSN-1-d in tab. 2) as the fitted data are compared with the mean value of all data to the values fitted. A negative value of R^2 indicates very poor correlation [20, 21]. Such fitting exercises were also discussed by Exner and Zvara [22].

For the tests in the shorter rig, hot smoke and flame might not spread up as a vertical channel flow. Therefore, the fitted curves deviated more from experiments. However, curve 4 on exact solution of the thermal equation gives better results. For the tests in the taller rig, fitted curves agreed with measurements better as hot smoke and flame are more likely to move up as a channel flow. Correlation coefficient R^2 for curve 4 can be up to 0.98 for tests DSN-1-b and DSN-1-c as shown in figs. 4(b) and (c). Note that R^2 for curves 1, 2 and 3 for these two

Table 2. Statistical analysis

Test number	Steady burning at time [s]	Curve 1					Curve 2				Curve 3				Curve 4				
		Fixed intercept			Fitted intercept														
		$\ln(T_0A_2)$ (measured)	C_1	R^2	$\ln(T_0A_1)$ (fitted)	C_1	R^2	A_2	B_2	C_2	R^2	A_3	B_3	C_3	R^2	A_4	B_4	C_4	C_5	R^2
DS-1-a	300	5.298	–0.463	0.87	5.308	–0.477	0.87	0.74	0.11	–0.99	0.72	0.66	0.17	0.73	0.88	0.64	0.03	–0.64	1.97	0.44
DS-1-b	300	5.004	–0.130	0.39	5.112	–0.281	0.66	0.54	0.02	–1.70	0.55	0.54	–0.08	0.11	0.64	0.51	0.03	–0.28	0.00	0.63
DS-1-c	400	5.623	–0.536	0.74	5.537	–0.415	0.84	0.85	0.07	–1.50	0.65	0.85	–0.06	0.37	0.86	0.87	–0.03	–0.39	0.30	0.85
DS-1-d	300	5.481	–0.408	0.44	5.399	–0.294	0.56	0.80	0.11	–0.93	0.49	0.73	–0.03	0.28	0.63	0.75	–0.03	–0.29	0.07	0.63
DS-2-a	200	5.921	–0.521	0.80	5.854	–0.428	0.86	1.18	0.11	–1.42	0.68	1.16	–0.09	0.38	0.88	1.19	–0.04	–0.40	0.36	0.87
DS-2-b	300	5.422	–0.321	0.52	5.413	–0.308	0.53	0.84	0.14	–0.81	0.50	0.73	–0.06	0.22	0.58	0.73	0.00	–0.40	–14.42	0.48
DSN-1-a	550	4.536	–0.508	0.84	4.536	–0.510	0.84	0.46	0.16	–0.53	0.74	0.31	0.00009	0.51	0.84	0.22	0.11	–0.11	–3.10	0.90
DSN-1-b	450	4.799	–0.571	0.86	4.736	–0.472	0.92	1.41	1.04	–0.12	0.88	0.38	0.00001	0.47	0.92	0.12	0.28	0.48	–1.40	0.98
DSN-1-c	400	4.758	–0.403	0.93	4.736	–0.379	0.94	1.95	1.57	–0.07	0.91	0.38	0.00007	0.38	0.94	0.02	0.37	1.41	–0.71	0.98
DSN-1-d	400	4.344	–0.734	–0.19	4.605	–0.330	0.16	4.79	4.60	–0.01	0.13	0.20	–0.00001	0.33	0.16	0.01	0.25	3.47	–1.76	0.94
DSN-1-e	200	4.748	–1.088	0.92	4.771	–1.127	0.92	5.58	5.22	–0.05	0.92	0.38	–0.22	0.34	0.93	–0.05	0.43	0.49	–0.78	0.93

tests are lower, say 0.92, 0.88, 0.92, respectively, for DSN-1-b; and 0.94, 0.91 and 0.94, respectively, for DSN-1-c. Note that the air temperature rises slightly while moving up the rig for curve 4. This might be due to vortex generated in the air cavity in the experiment. However, such effect cannot be predicted in the above thermal equation with parameters deduced from first principles. This should be explored in more detail.

In view of fig. 4(d) for test DSN-1-d, R^2 for curve 4 is 0.94 with fitting much better than the other three curves with very low R^2 down to 0.13. Therefore, including the second-order derivative in the thermal eq. (9) is important in modeling the vertical channel flow for narrow cavity. It is dangerous to neglect it as shown by results in curve 1.

In view of eq. (28c), the intercept is $\ell n\Delta T_{CJ}$ and the slope is β_1/H. From eq. (10) for β_1, the slope β_1/H is:

$$\frac{\beta_1}{H} = \frac{h}{4GI\rho_0 C_p T_0} \qquad (34)$$

Note that h is the heat transfer coefficient, G is a geometrical factor given by eq. (5) and I depends on initial conditions and channel geometry given by eq. (8). The two parameters h and G can be taken as constants for the same DSF rig. Parameter I is related to v and T which depend on the fire size of the room chamber adjacent to it.

In the tests with the shorter rig DS of 6 m tall, the fire size was the same as for those tests useful for the analysis in vertical channel flow. Similarly, tests DSN-1-a to DSN-1-e in the tests with the taller rig DSN of 15 m tall with 1 m cavity depth are also useful for justifying vertical channel flow.

Values of γ and β_1 can be deduced from the fitted slopes of the curves. The geometrical factor G and fire factor I can then be determined from eq. (10) using β_1. Value of β_1 from fitted intercepts for tests in rig DS with narrow cavity depth over the eight tests varies from 0.172 to 0.477, with a mean of 0.318. In view of eq. (10), GI would be about $2D$, giving I or v/T in eq. (9) of about 10^{-4} mK/s. The value is reasonable for hot gases moving up slowly with speed down to 0.1 m/s and T up to 1000 K. γ can be determined from eq. (13) on γ/β_1 to give $4G/HNu$.

For D of 1 m and f_w of 1 m, G is 1 m. T_0 is about 300 K and H is 15 m. Value of γ/β_1 is about 0.000266667, much less than 1.

To estimate actual values of γ and β_1, values of v and I have to be calculated. Value of v can be very slow at 0.1 m/s or fast up to 1 m/s; and T is from 300 K to 1000 K. For I of 1/300, β_1 is 0.005977, γ is 0.000004782 for moving up a 6 m DSF rig; and 0.000001594 for another taller DSF rig of 15 m height. But for I of 0.1/1000, β_1 is 0.19925 and γ is 0.0001593 for the 6 m rig and 0.000053 for the 15 m rig. $1 - 4\gamma\beta_1$ is very close to 1 for reasonable values of I. However, in view of eq. (30) on curve 2, value of γ is far less than 1. These contradict with fitted values of C_2 shown in tab. 2. There is similar observation on C_3 for curve 3. Therefore, curves 1, 2, and 3 deduced from different approximations by taking out some terms in the key equation should be used carefully.

Conclusions

A simple mathematical model was developed to study the air temperature in the air cavity of a DSF. Full-scale burning tests were carried out in two DSF rigs of 6 m and 15 m tall. Average air temperatures in the façade cavity measured at different heights were used to justify the above equations using the method of least square fitting. The equations fitted well

to give the air temperature above the fire room for narrow cavity depth. Empirical expressions derived by the above methodology would be useful in fire hazard assessment for DSF. Air temperature estimated in the façade cavity can be applied to study thermal response of the two glass panes with different cavity gaps. Results with further experimental justification can be applied for setting up appropriate regulations.

Acknowledgment

The author would like to thank Professor K. Steemers in supervising the Ph. D. project at Cambridge.

Nomenclature

A – cross-sectional area of the façade rig, [m^2]
C_p – specific heat capacity of air, [Jkg^{-1}K^{-1}]
D – cavity depth of the façade, [m]
f_w – opening window flame width, [m]
G – geometrical factor, [–]
H – height of façade rig, [m]
h – heat transfer coefficient, [Wm^{-2}K^{-1}]
I – ratio on upward air velocity and air temperature, [–]
k – thermal conductivity, [Wm^{-1}K^{-1}]
M – molar mass, [kg]
$\dot{m}$ – mass flow rate, [kgs^{-1}]
Nu – Nusselt number, [–]
P_0 – ambient air pressure, [Pa]
R – gas constant, [–]
R^* – given by RM, [–]
R^2 – coefficient of determination, [–]
T – air temperature, [K]
T_0 – initial and ambient air temperature, [K]
T_{ci} – ceiling jet temperature, [K]
ΔT – temperature rise of hot air, [K]
ΔT_{CJ} – ceiling jet temperature rise, [K]
v – upward air velocity, [ms^{-1}]
W_1 – width of the channel flow, [m]
Y – dimensionless vertical height, [–]
y – vertical height above fire room ceiling, [m]

Greek symbols

β_1 – a parameter in the thermal equation, [–]
γ – a parameter in the thermal equation, [–]
θ – ratio of temperature rise to ambient air temperature, [–]
θ_0 – boundary condition of θ, [–]
ρ – air density, [kgm^{-3}]
ϕ – ratio of density difference to ambient air density, [–]
ρ_0 – ambient air density, [kgm^{-3}]

References

[1] Button, D., Pye, B., *Glass in Building: A Guide to Modern Architectural Glass Performance*, Pilkington, Oxford, UK, 1993
[2] Blomsterberg, Å., *et al*., *BESTFAÇADE: Best Practice for Double Skin Façades – Literature*, EIE/04/135/S07.38652, 2007. www.bestfacade.com
[3] Lstiburek, J. W., Why Green Can be Wash, *ASHRAE Journal*, *50* (2008), 11, pp. 28-36
[4] Sinclair, R., *et al*., Ventilating Façades, *ASHRAE Journal*, *51* (2009), 4, pp. 16-27
[5] Chow, W. K., Fire Safety in Green or Sustainable Buildings: Application of the Fire Engineering Approach in Hong Kong, *Architectural Science Review*, *46* (2003), 3, pp. 297-303
[6] Hulin, K., To Glaze or Not to Glaze, *Fire Prevention and Fire Engineers Journal*, Fire Summit Special Issue, (2007), pp. 47-49
[7] ***, Fire Services Department, *Codes of Practice for Minimum Fire Service Installations and Equipment and Inspection and Testing of Installations and Equipment*, Hong Kong, 2005
[8] Himoto, K., *et al*., Modeling the Trajectory of Window Flames with Regard to Flow Attachment to the Adjacent Wall, *Fire Safety Journal*, *44* (2009), 2, pp. 250-258
[9] Chow, W. K., Hung, W. Y., Effect of Cavity Depth on Smoke Spreading of Double-Skin Façade, *Building and Environment*, *41* (2006), 7, pp. 970-979
[10] Chow, W. K., *et al*., Experimental Study on Smoke Movement Leading to Glass Damages in Double--Skinned Façade, *Construction and Building Materials*, *21* (2007), 3, pp. 556-566
[11] Chow, C. L., Assessment of Fire Hazard on Glass Buildings with an Emphasis on Double-Skin Façades, Ph. D. dissertation, Department of Architecture, University of Cambridge, UK, 2009

[12] Chow, C. L., Numerical Simulations on Airflow to the Double-Skin Façade Cavity by an Adjacent Room Fire, *ASME 2010 International Mechanical Engineering Congress & Exposition*, 2010, Vancouver, B. C., Canada, Paper No. IMECE2010-37478
[13] Zukoski, E. E., A Review of Flows Driven by Natural Convection in Adiabatic Shafts, NIST-GCR-95-679, Gaithersburg, Md., USA, 1995
[14] Tanaka, T., *et al*., Investigation into Travel Time of Buoyant Fire Plume Fronts, *Proceedings,* First International Symposium on Engineering Performance-Based Fire Codes, Hong Kong, China, 1998, pp. 220-228
[15] Benedict, N. L., Buoyant Flows in Vertical Channels Relating to Smoke Movement in High-Rise Building Fires, Ph. D. thesis, California Institute of Technology, Pasadena, Cal., USA, 1999
[16] Mercier, G. P., Jaluria, Y., Fire-Induced Flow of Smoke and Hot Gases in Open Vertical Enclosures, *Experimental Thermal and Fluid Science*, *19* (1999), 1, pp. 77-84
[17] Chew, M. Y. L., Liew, P. H., Smoke Movement in Atrium Buildings, *International Journal on Engineering Performance-Based Fire Codes*, *2* (2000), 2, pp. 68-76
[18] Sun, X. Q., *et al*., One-Dimensional Smoke Movement in Vertical Open Shafts at Steady State: Theoretical Prediction and Experimental Verification, *Proceedings,* ASME Summer Heat Transfer Conference, Jacksonville, Fla., USA, 2008
[19] Atreya, A., Convective Heat Transfer, in: *SFPE Handbook of Fire Protection Engineering*, 3rd ed., NFPA-SFPE Quincy, Mass., USA, 2002
[20] Kirkup, L., *Data Analysis with Excel – An Introduction for Physical Scientists,* Cambridge University Press, Cambridge, UK, 2002
[21] Walpole, R. E., *et al*., *Probability & Statistics for Engineers & Scientists,* 8th ed., Pearson Prentice-Hall, Upper Saddle River, N. J., USA, 2007
[22] Exner, O., Zvara, K., Coefficient of Determination in Some Atypical Situations: Use in Chemical Correlation Analysis, *Journal of Physical Organic Chemistry*, *12* (1999), 1, pp. 151-156

Paper submitted: September 18, 2011
Paper revised: April 13, 2012
Paper accepted: April 28, 2012